Supplementary information for "Determination of Electric-Field, Magnetic-Field, and Electric-Current Distributions of Infrared Optical Antennas: A Near-Field Optical Vector Network Analyzer"

Robert L. Olmon[1], Matthias Rang[1],* Peter M. Krenz[2], Brian A. Lail[3], Laxmikant V. Saraf[4], Glenn D. Boreman[2], and Markus B. Raschke[1,†]

[1]*Department of Physics, and JILA, University of Colorado at Boulder, Colorado 80309, USA*

[2]*Center for Research and Education in Optics and Lasers (CREOL), University of Central Florida, Orlando, Florida 32816, USA and*

[3]*Deptartment of Electrical and Computer Engineering, Florida Institute of Technology, Melbourne, Florida 32901, USA*

[4]*Environmental Molecular Sciences Laboratory, Pacific Northwest National Laboratory, Richland, Washington 99352, USA*

The performance of the vector near-field imaging method presented in the main text is sensitive to the properties of the probe tip. Here we describe further details of the fabrication process and results of simulations regarding tip scattering with and without the Pt probe antenna. We also provide further procedural details regarding the vector field measurement with respect to individual field components and spatial resolution. Last, discussion of the method for magnetic field and current density determination is provided.

PROBE FABRICATION

The very tip apex of a commercial atomic force microscope (AFM) Si probe tip (AdvancedTEC NC, $\rho = 0.01 \sim 0.025\,\Omega$·cm) is cut off using a Ga^+ focused ion beam (FIB) (FEI Helios 600, Ga^+ current 90 pA, beam energy 30 keV) to create a well defined ∼200 nm wide plateau [1]. The plateau is oriented at an angle of 60° with respect to the tip axis as required by the *s*-SNOM configuration to ensure that its orientation is parallel with respect to the scanning plane. A ∼ 50 nm thick platelet of Pt is subsequently deposited onto the plateau using *in situ* electron beam assisted nanoscale chemical vapor deposition (nano-CVD) with a $CH_3CpPt(CH_3)_3$ (trimethylplatinum-methylcyclopentadienyl) precursor as the platinum source (electron beam current ∼100 pA) [2]. This platelet probe antenna, with dimensions of $\sim \lambda/50$ is sub-resonant compared to the excitation wavelength of $\lambda = 10.6$ μm used in the experiment. It can be considered a low-power Rayleigh point dipole emitter, thus minimally perturbing the antenna near-field to be investigated, similar to the use of a bare Si tip [3]. Moreover, with antenna illumination perpendicular to the tip axis, thus resonantly exciting the sample but not the probe tip, undesired coupling effects between the tip and the sample are expected to be minimal for both detection polarization configurations. This is in contrast to a tip-parallel illumination and detection configuration where strong tip-sample dipole-dipole coupling can distort the intrinsic antenna field thus making the interpretation of the recovered signal difficult [4].

TIP SIMULATIONS

To aid in the probe design, the optical response characteristics of the original Si bulk probe and the modified nanocomposite Pt-Si probe are simulated based on the finite element method (HFSS, Ansoft LLC). The bulk tip is modeled as a Si-cone oriented in the *z*-direction with a full taper angle of 20°, terminated by a hemispherical apex with 10 nm radius. For the modified tip, the cone is truncated and capped with a cylindrical Pt layer in the *x*-*y* plane, 25 nm thick and 100 nm in diameter. A plane wave is incident propagating in the *y*-direction with a field strength of 1 V/m, polarized in either the *x*- or the *z*-direction. It should be mentioned that the tip used in the experiment is covered by a native SiO_2 surface layer [5]. That thin layer, neglected in the simulation, is not expected to alter the general conclusions drawn from the simulation.

Figure 1 (Supplemental) shows the expected optical response for parallel (a and b) and perpendicular (c and d) illumination with respect to the tip axis. While the unmodified bulk tip shows a strong non-plasmonic antenna-type response under tip-parallel excitation with an enhancement factor of 24 at the apex (a), its response under tip-perpendicular illumination is negligible (c). The bulk tip is thus largely insensitive with respect to the perpendicular vector component $E_\perp$. On the other hand, the Pt-terminated tip produces an enhanced field in response to both perpendicular (d) and parallel polarization (b) with the latter attenuated by only 17% compared to the bulk tip thus giving rise to increased scattering via the induced dipole at the apex subject to the $E_\perp$ near-field component of the antenna being probed.

FIELD MEASUREMENT

Despite their simplicity, fundamental questions regarding linear antenna scaling behavior still remain open, in particular in the mid-IR spectral range related to the transition between the low-energy Hagen-Rubens regime ($\omega \ll 1/\tau_{Drude}$) characterized by high conductivity and low absorption, and the relaxation regime $1/\tau < \omega < \omega_{pl}$ with plasma frequency ω_{pl} [6]. Yet with a Drude relaxation time $\tau_{Drude} \simeq 30$ fs for Au corresponding to the optical cycle period of $\lambda \simeq 10$ μm radiation, devices operating in the mid-IR retain the ability to

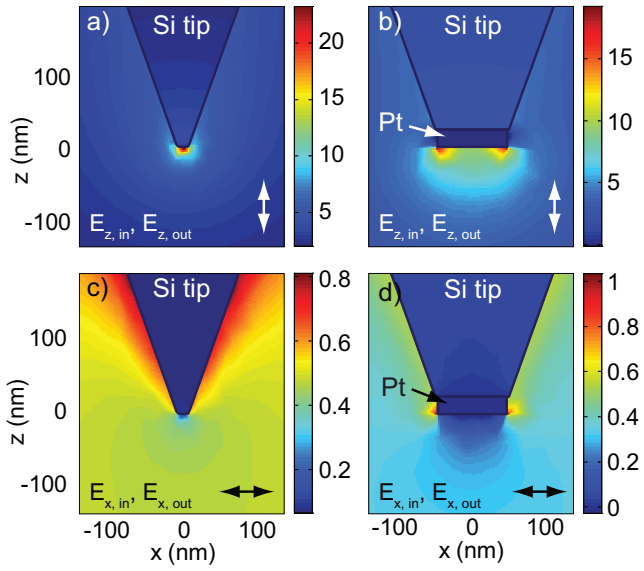

FIG. 1. (Supplemental) The simulated optical electric field response $|\boldsymbol{E}_\mathrm{i}|$ (i $= x,z$) for parallel (a and b) and perpendicular (c and d) illumination ($\lambda = 10.6$ μm) with respect to the tip axis for a Si bulk tip (a and c) and the modified probe tip (b and d) given in V/m. The image is shown at the time in the optical cycle of highest field amplitude. A dipolar response is clearly seen in the modified tip.

sustain surface plasmon polaritons, with enhanced propagation length [7].

The linear Au dimer antennas are fabricated on a Si substrate by electron beam lithography and lift-off. The nominal size of each antenna is 1.7 μm × 110 nm with a height of 70 nm.

A carefully balanced weak homodyne reference field enables the assignment of the near-field phase at each sampling point. The relative temporal phase of the detected near-field can be adjusted from 0 to 2π with the reference mirror. Spatial variation in phase can be understood as the direction of the measured near-field vector at each point with respect to the direction of the reference field vector at a specific time. For the measurements shown, the relative phase was adjusted for maximum signal amplification. The spatial phase variation is observed separately for the two measured near-field components E_y and E_z. While for the E_z component, a π-phase change is observed between the endpoints of each antenna, the E_y field amplification is positive throughout with respect to the near-field on the surrounding Si, indicating a spatially homogeneous phase for E_y as expected for the coupled dipoles. Note that while the phase of the linear antenna assumes one of two values separated by π, the phase can be more complicated in general, e.g. for superposition of resonances, or retardation as a result of the driving field across the structure. In that case, the full temporal phase evolution at each sampling point must also be measured in order to reconstruct the electric field with full spatial and temporal information. The combination of the two field components yields the complete vector field with the relative amplitude between E_y and E_z established from relative x_{in}/x_{out} and z_{in}/z_{out} polarization combinations in far-field scattering.

From E-field data of Fig. 2 (main text), field enhancement, estimated from comparison with off-resonant signal levels is 15 ± 5 at the gap and 11 ± 3 at the outer terminals for E_y, and 32 ± 18 near the gap and 17 ± 10 at the outer terminals for E_z with spatial $1/\mathrm{e}$ decay length of 38 nm and 33 nm, respectively, in good agreement with theory and related experiments [7, 8].

Though the modified probe tip apex has a diameter of $\sim$ 200 nm, a spatial resolution of up to ~ 40 nm as been obtained in the near-field images. With the probe tip under a slight tilt, the near-sample edge of the triangular Pt platelet ultimately defines the resolution and sensitivity. With a tilt angle of just a few degrees, depolarization of the scattered signal is still found to be negligible.

DETERMINATION OF MAGNETIC FIELD AND CURRENT FROM ELECTRIC FIELD DATA

In general, the electric vector field $\boldsymbol{E}$ and magnetic field $\boldsymbol{H}$ of the time-varying optical electromagnetic wave are related by Faraday's Law.

$$\boldsymbol{H} = -\frac{\mathrm{i}}{\omega\mu_0}\frac{\partial \boldsymbol{B}}{\partial t} = \frac{\mathrm{i}}{\omega\mu_0}\nabla\times\boldsymbol{E}. \tag{1}$$

Here we use the constitutive relation $\boldsymbol{B} = \mu_0\boldsymbol{H}$ and the fact that the time derivative of a time-harmonic wave can be represented instead as a multiplication by $\mathrm{i}\omega$ where ω is the frequency of the wave.

Using the geometry from Fig. 1 in the main text, the antenna near-field is measured in the mirror plane defined by $x = 0$. This simplifies the numerical curl operation. In this geometry, the magnetic field consists of only a x-component produced from the spatial derivatives of the electric field in the y- and z-directions, and Eq. 1 simplifies to

$$H_x = \frac{\mathrm{i}}{\omega\mu_0}\left(\frac{\partial E_\mathrm{z}}{\partial y} - \frac{\partial E_\mathrm{y}}{\partial z}\right). \tag{2}$$

A magnetic-field enhancement $|\boldsymbol{H}_{nf}|/|\boldsymbol{H}_{inc}|$ of ~ 16 can be estimated with the incident field approximated by $|H_x(z = 180\ \mathrm{nm})|$ normalized to 1. This agrees with the corresponding value of ~ 15 from theory considering $|\boldsymbol{H}_{inc}| = 2.7$ mA/m ($\equiv |\boldsymbol{E}_{inc}| = 1$V/m). The electric field in space $\boldsymbol{E}(\boldsymbol{r})$ and the associated current density $\boldsymbol{J}(\boldsymbol{r'})$ of a conductor are related through the magnetic vector potential $\boldsymbol{A}(\boldsymbol{r})$ with $\boldsymbol{B}(\boldsymbol{r}) = \nabla\times\boldsymbol{A}(\boldsymbol{r})$. Approximating $\boldsymbol{J}$ as a line current, $I(y')$ is determined directly from the measured electric near-field antenna-parallel component E_y and can be obtained as the solution to Hallén's integral equation which relates $E_y(y)$ to $I(y')$ through $\boldsymbol{A}(\boldsymbol{r})$ at the antenna surface,

$$\frac{\mu_0}{4\pi}\int_{-l/2}^{l/2} I(y')G(y-y')dy' = \mathrm{i}\omega\mu_0\varepsilon_0(\partial_y^2 + k^2)^{-1}E_y(y) \tag{3}$$

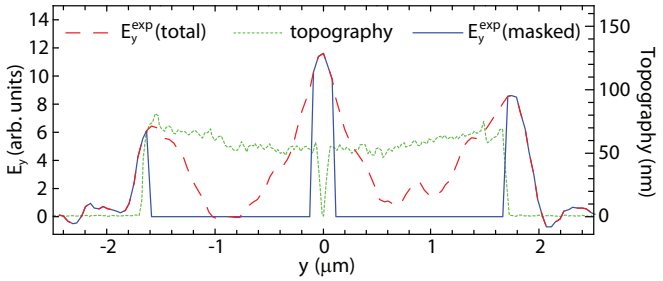

FIG. 2. (Supplemental) E_y is masked above the surface of the antenna to diminish possible distortions of the dipole field due to scattering of fields enhanced by surface roughness. The mask position is defined by the topography as measured using an unmodified probe tip.

with antenna length l in wavelengths, $k^2 = \omega^2/\mu_0\varepsilon_0$, and kernel $G(y-y')$, a geometrical parameter related to the distance from each point of $I(y')$ to each point of $E_y(y,z)$ [9, 10]. This equation is solved numerically by the method of moments with a pulse-function basis with point matching using MATLAB following Ref. [10].

The resulting $I(y)$ (Fig. 4 (a) in the main text), while exhibiting a quasi-sinusoidal distribution as expected, shows no discernible signature of the expected dipole coupling. The possibility of distortions in the measured in-plane near-field due to, e.g., contributions of fields locally enhanced by surface roughness of the metal prompts an alternative analysis. Masking the field in the regions above the metal surface diminishes any deleterious effects of possible extraneous light scattering from surface roughness on the current reconstruction, yet maintains the longer range near-field characteristics arising from the macroscopic delocalized antenna mode. Figure 2 (supplemental) shows E_y with and without the mask defined by the superimposed topography as measured with an unmodified probe tip. These fields are used to determine the current distributions as shown in Fig. 4 (a) (from E_y(total)) and Fig. 4 (b) (from E_y(masked)) in the main text.

For comparison, the conduction current is also derived from the magnetic field data. Near the conductor surface, the underlying source conduction current density is approximately $\boldsymbol{J} = \boldsymbol{\nabla} \times \boldsymbol{H}$. With H_x given above, considering that the conduction current is largely one-dimensional and dominated by the y-component for the linear antenna geometry studied, the curl equation can be simplified to

$$J(y) = -\frac{\partial}{\partial z} H_x(y,z). \tag{4}$$

This method qualitatively reproduces the current peak shift seen when the masked field is used. However, this current reconstruction approach involves several derivatives from the original $\boldsymbol{E}$ data, resulting in amplification of noise compared to the method of moments. Nevertheless, it does provide an additional check on the expected $I(y)$ distribution as shown in the main text in Fig. 4(c).

Thus if $\boldsymbol{E}$ is known in sufficient detail, one may calculate the associated $\boldsymbol{H}$ and $\boldsymbol{J}$. Though simplified here for the case of a linear antenna geometry, these operations are general and can readily be extended for the determination of magnetic field and current from 3D near-field data for arbitrary antenna geometries.

* Present address: Forschungsinstitut am Goetheanum, CH 4143 Dornach, Switzerland

† markus.raschke@colorado.edu

[1] L. A. Giannuzzi and F. A. Stevie, *Introduction to focused ion beams: Instrumentation, theory, techniques and practice* (Springer, 2005).

[2] W. F. van Dorp and C. W. Hagen, J. Appl. Phys. **104**, 081301 (2008).

[3] M. Schnell, A. Garcia-Etxarri, A. J. Huber, K. B. Crozier, A. Borisov, J. Aizpurua, and R. Hillenbrand, J. Phys. Chem. C. **114**, 7341 (2010).

[4] R. Esteban, R. Vogelgesang, J. Dorfmuller, A. Dmitriev, C. Rockstuhl, C. Etrich, K. Kern, Nano Lett. **8**, 3155-3159 (2008).

[5] D. Haefliger, J. M. Plitzko, and R. Hillenbrand, Appl. Phys. Lett. **85**, 4466 (2004).

[6] M. Dressel and G. Grüner, *Electrodynamics of Solids* (Cambridge University Press, Cambridge, England, 2002).

[7] A. C. Jones et al., R. L. Olmon, S. E. Skrabalak, B. J. Wiley, Y. N. Xia, and M. B. Raschke, Nano Lett. **9**, 2553 (2009).

[8] F. Neubrech, T. Kolb, R. Lovrincic, G. Fahsold, A. Pucci, J. Aizpurua, T. W. Cornelius, M. E. Toimil-Molares, R. Neumann, and S. Karim, Appl. Phys. Lett. **89**, 253104 (2006).

[9] C. A. Balanis, *Antenna Theory: Analysis and Design* (Wiley, 1997).

[10] S. J. Orfanidis, *Electromagnetic Waves and Antennas* (www.ece.rutgers.edu/~orfanidi/ewa, 2008).